

## DENSITIES AND ECCENTRICITIES OF 139 *KEPLER* PLANETS FROM TRANSIT TIME VARIATIONS

SAM HADDEN, YORAM LITHWICK

Department of Physics & Astronomy, Northwestern University, Evanston, IL 60208, USA & Center for Interdisciplinary Exploration and Research in Astrophysics (CIERA)

*Draft version April 9, 2014*

### ABSTRACT

We extract densities and eccentricities of 139 sub-Jovian planets by analyzing transit time variations (TTVs) obtained by the *Kepler* mission through Quarter 12. We partially circumvent the degeneracies that plague TTV inversion with the help of an analytical formula for the TTV. From the observed TTV phases, we find that most of these planets have eccentricities of order a few percent. More precisely, the r.m.s. eccentricity is  $0.018^{+0.005}_{-0.004}$ , and planets smaller than  $2.5R_{\oplus}$  are around twice as eccentric as those bigger than  $2.5R_{\oplus}$ . We also find a best-fit density-radius relationship  $\rho \approx 3 \text{ g/cm}^3 \times (R/3R_{\oplus})^{-2.3}$  for the 56 planets that likely have small eccentricity and hence small statistical correction to their masses. Many planets larger than  $2.5R_{\oplus}$  are less dense than water, implying that their radii are largely set by a massive hydrogen atmosphere.

*Subject headings:* planets and satellites:composition, planets and satellites:dynamical evolution and stability

### 1. INTRODUCTION

The *Kepler* telescope has provided an unprecedented look into the world of extrasolar planetary systems. It has detected the transits of thousands of planetary candidates, most of which are smaller than Neptune and orbit with periods  $\lesssim 100$  days (Batalha et al. 2013; Borucki et al. 2011, 2010). A transiting planet’s orbital period is trivially deduced from the time between transits, and its radius from the depth of transit. But its other physical properties are much more difficult to obtain, including mass and eccentricity.<sup>1</sup> Knowledge of a planet’s mass—and hence density—can inform us about its composition; and knowledge of its eccentricity can constrain its dynamical history. Both are key clues towards understanding how the surprising planetary systems discovered by *Kepler* formed and evolved.

A handful of *Kepler* planets have had their masses measured with radial velocity (RV) follow-up (Koch et al. 2010; Batalha et al. 2011; Cochran et al. 2011; Gautier et al. 2012; Gilliland et al. 2013).<sup>2</sup> But RV measurements are very difficult to obtain for the bulk of low-mass *Kepler* candidates. In multi-planet systems, one can take advantage of the fact that mutual gravitational perturbations alter the times of transit. If these transit time variations (TTVs) can be detected, they can be used to characterize planets (Agol et al. 2005; Holman & Murray 2005; Steffen et al. 2013, 2012; Fabrycky et al. 2012; Nesvorný et al. 2012; Lithwick et al. 2012; Xie 2013). TTVs are exquisitely sensitive to the planets’ masses and eccentricities, and can probe planets that are too far from

their star or too small to yield a detectable RV signal. But they depend on planet properties in a non-trivial way and can suffer from important degeneracies, making it a challenge to invert the TTV signal to infer the planets’ properties.

To overcome this challenge, we perform the inversion with the help of simple analytical formulae for the TTV, derived in Lithwick et al. (2012). We focus on near-resonant pairs, which have particularly large TTV signals. To a good approximation, the TTV of each planet in such a pair is sinusoidal, with period  $P'/|j\Delta|$  (which we call the “superperiod”), where  $\Delta = P'(j-1)/(Pj) - 1$  is the normalized distance to the nearest  $j : j-1$  resonance, and  $P$  and  $P'$  are the average orbital periods of the inner and outer planet.<sup>3</sup> Thus we write the deviation of the transit times from perfect periodicity as the imaginary part of

$$V \times e^{i(2\pi j\Delta/P')t}, \quad (1)$$

for the inner planet, and similarly for the outer with  $V \rightarrow V'$ . The complex amplitudes are set by the planets’ masses and eccentricities via

$$\begin{aligned} V &= \frac{P}{\pi} \frac{\mu'}{j^{2/3}(j-1)^{1/3}\Delta} \left( -f - \frac{3}{2\Delta} Z_{\text{free}}^* \right) \\ V' &= \frac{P'}{\pi} \frac{\mu}{j\Delta} \left( -g + \frac{3}{2\Delta} Z_{\text{free}} \right) \end{aligned} \quad (2)$$

where  $\mu$  is the planet-to-star mass ratio,  $f$  and  $g$  are order-unity numbers listed in Table 3 of Lithwick et al. (2012), and  $Z_{\text{free}} = fz + gz'$  is a linear combination of the complex free eccentricities ( $z = ee^{i\varpi}$ ) of the two planets.<sup>4</sup>

<sup>3</sup> We follow the convention of using primes to denote quantities corresponding to the outer planet.

<sup>4</sup> The typical free eccentricities that we deduce in this paper are much larger than the planets’ forced eccentricities, and hence nearly equal to the total eccentricities. We shall therefore call the free eccentricity simply the eccentricity, with the understanding that it is really the free eccentricity that is deduced from TTV measurements.

<sup>1</sup> Inclinations can be deduced statistically from the relative numbers of transiting planets in different systems. The inclination dispersion is found to be very small—a few degrees (e.g., Lissauer et al. 2011a; Figueira et al. 2012; Tremaine & Dong 2012; Fang & Margot 2012; Johansen et al. 2012; Weissbein et al. 2012). There may be a second population of highly inclined systems, although that is strongly degenerate with the spacing distribution (Lissauer et al. 2011a).

<sup>2</sup> After this paper was submitted, Marcy et al. (2014) reported an additional 16 *Kepler* planets with RV-measured masses.

In this paper, we first extract the amplitudes ( $V$  and  $V'$ ) of 139 *Kepler* planet candidates from the transit times up to Quarter 12 published in Mazeh et al. (2013). We then invert Eqs. (2) to infer the eccentricities and masses (and hence densities) of the planets. Because of degeneracies inherent in Eqs. (2), one must make use of statistical arguments to effect the inversion. The approach we take here is largely similar to that in Lithwick et al. (2012) and Wu & Lithwick (2013), who analyze 22 *Kepler* pairs up to Quarter 6.

## 2. EXTRACTING THE TTV AMPLITUDES

Mazeh et al. (2013) catalog the transit times of 1960 KOIs with high SNR, using *Kepler* data up to Q12. We select planet pairs from their catalog that lie sufficiently close to the first-order resonances 2:1, 3:2, 4:3, or 5:4, such that  $|\Delta| < 0.06$ . This reduces the sample size to 133 pairs, which is around a third of all pairs of adjacent planets in their list. For each planet in a pair, we fit the Mazeh et al. (2013) transit times with a sum of two components: one linear in time and the other sinusoidal. The period of the latter is enforced to be the pair’s superperiod ( $= P'/|j\Delta|$ ). Since the superperiod depends on the individual planet periods, which in turn depend on the linear components of the fits, we perform a non-linear Levenberg-Marquardt fit. In systems with three or more planets, the TTV of a planet with two perturbers is nearly a linear sum of the TTV induced by each perturber alone (at the corresponding superperiod). Therefore for such systems, we fit the TTVs for all expected sinusoidal components simultaneously.<sup>5</sup>

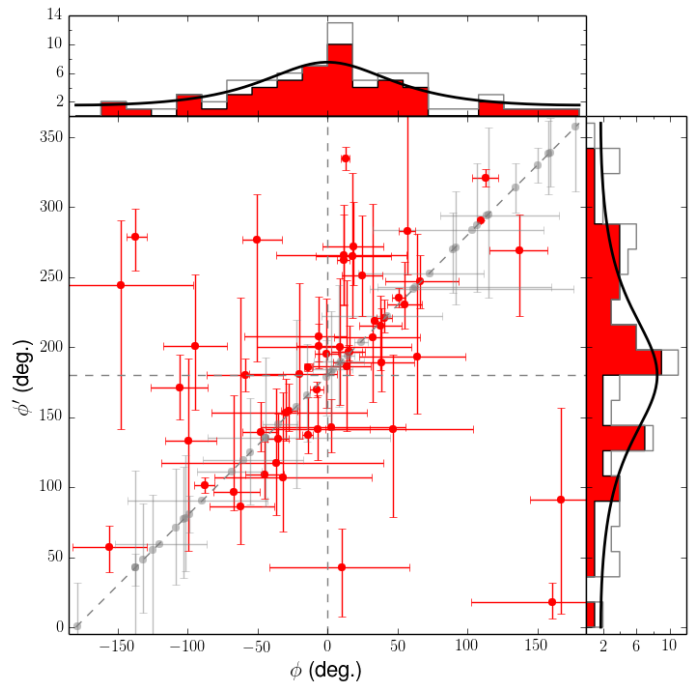
Table 1 lists 95 planet pairs in which one or both partners have “well-detected” TTV’s, which we take to mean that their TTV amplitudes are inconsistent with 0 at the predicted superperiod with 68% confidence, based on the covariance matrix generated by the fit. The table also gives the values of  $V$  and  $V'$  (amplitudes and phases) and errors (at 68% confidence). In total, there are 149 well-detected TTV’s in the table, which we refer to as our primary sample. After accounting for repeated planets (from triples), our primary sample is comprised of 139 distinct planets.

Table 1 includes 21 of the pairs analyzed previously over a shorter time baseline (Lithwick et al. 2012; Wu & Lithwick 2013). Xie (2014) extracts the amplitudes for 15 pairs after determining the transit times directly from the Kepler light curves. Seven of his pairs overlap with ones in our list; our amplitudes largely agree with his.

## 3. ECCENTRICITIES AND MASSES FROM TTV

We seek to extract the planets’ eccentricities and masses from the values of  $V$  and  $V'$  by inverting Eqs. (2). However, there is a strong degeneracy: for any pair, one may scale down the masses without affecting the TTV, as long as one correspondingly scales up the eccentrici-

<sup>5</sup> Three of the triples require special treatment because the superperiod of the outer pair is nearly the same as that of the inner pair. For these “degenerate triples,” we exclude the middle planet’s TTV (as marked by a dash in Table 1), because the effect of its two partners cannot be disentangled. In addition, we exclude the following systems from further consideration: KOIs 500 and 730 because of multiple degeneracies; KOIs 262 and 1858 because their expected superperiods are too long; and KOI738 because it is strongly perturbed by the 9:7 resonance.



**Figure 1.** TTV phases of planets in our primary sample (Table 1). The red points denote the 54 pairs in which both planets have well-measured TTVs, and show the inner planet’s vs. outer planet’s phase. The grey points denote the 41 pairs that have a single measured TTV, such that each point (with error bar) corresponds to the detected planet. Error bars denote the 68% confidence interval. The side panels show histograms of the red points (shaded histograms) and grey points (unshaded). Nearly all the red points lie along the dashed diagonal line, i.e., the inner and outer planets have anticorrelated phases, as implied by Eqs. (2). Furthermore, the points cluster near, but not always at, the point  $(0^\circ, 180^\circ)$ . This implies both that  $e \lesssim |\Delta| \sim 0.02$  and that it is not true that  $e \ll |\Delta|$ . The solid curves in the side panels show the phase distribution produced by our maximum likelihood fit eccentricity distribution with  $\sigma_e = 0.018$ , after folding in the observed values of  $\Delta$ .

ties. Nonetheless, this degeneracy can be partially lifted with a large sample of TTVs. We proceed in two steps.

### 3.1. Eccentricity Distribution

In the first step, we work with the *phases* of  $V$  and  $V'$  to determine the distribution of eccentricities. The phases depend only on the eccentricities, not the masses (Eqs. (2)). For a single planet pair, the phases cannot be used to infer the eccentricities because they depend on the unknown orientation of the planets’ Keplerian ellipses ( $\varpi$ ).<sup>6</sup> But the orientation should be random with respect to the line of sight, i.e., the complex phase of  $Z_{\text{free}}$  should be random. Therefore Eqs. (2) imply that if all the planets have sufficiently large  $e$  ( $e \gg |\Delta|$ ), the TTV phases will be uniformly distributed between  $-180^\circ$  and  $180^\circ$ . Conversely, if the planets have small  $e$  then the phases of the inner planets will all be zero, and those

<sup>6</sup> In principal, the two TTV amplitudes and two phases can yield 4 quantities: two planet masses and the real and imaginary components of the combined free eccentricity,  $Z_{\text{free}}$ . However, in most systems the inner and outer planets’ TTVs should be nearly perfectly out of phase with one another—whether  $|Z_{\text{free}}/\Delta| \gg 1$  or  $\ll 1$ . Hence there are really only three observed quantities given the typical noise in observed TTVs.

of the outer will be  $180^\circ$ .<sup>7</sup>

Figure 1 displays the phases of our pairs with well-detected TTV's, along with histograms of the inner and outer planets' TTV phases. The phases unambiguously cluster near  $(0^\circ, 180^\circ)$  indicating that the vast majority of the planets have  $e \lesssim |\Delta|$ , i.e.,  $e \lesssim 0.02$  using the typical value of  $|\Delta|$ . But many phases differ markedly from  $(0^\circ, 180^\circ)$ , indicating that many planets cannot have  $e \ll 0.02$ . These inferences are robust, essentially independent of any assumption.

To be more precise, we assume that the eccentricities of the planets are drawn from the same underlying distribution, which we take to be Rayleigh with scale parameter  $\sigma_e$ .<sup>8</sup> We then determine  $\sigma_e$  by maximizing the total likelihood of the observed phases under the assumed eccentricity distribution. The likelihood that a given planet in our sample has observed TTV phase  $\phi_{\text{obs}}$  is the convolution

$$l(\phi_{\text{obs}}|\sigma_e) = \int P(\phi|\sigma_e) e^{-(\phi-\phi_{\text{obs}})^2/(2\sigma_\phi^2)} d\phi, \quad (3)$$

where  $\phi$  is its true TTV phase; the first factor in the integrand is the probability that the phase as determined by Eqs. (2) is  $\phi$ , assuming that the planets'  $e$ 's are randomly drawn from the Rayleigh distribution; and the second factor is the probability that the noise generates the observed phase from  $\phi$ , where  $\sigma_\phi$  is the 68% confidence error on  $\phi_{\text{obs}}$  (averaging the asymmetric error bars). Note that  $P(\phi|\sigma_e)$  also depends on the (known) value of  $\Delta$  but not on the masses. We compute the total likelihood by multiplying together the likelihoods for all pairs, where the phase for a pair is taken to be the phase of its inner planet, which in turn is taken to be either  $\phi$  or  $\phi' - 180^\circ$  depending on which planet has the smaller phase error bar. Maximizing the total likelihood, we find

$$\sigma_e = 0.018_{-0.004}^{+0.005}, \quad (4)$$

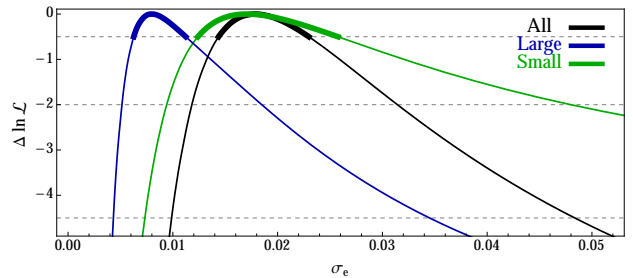
where the error bars delimit a decrease in the total likelihood by  $\Delta \ln \mathcal{L} = -0.5$  which would constitute the 68% confidence interval for a normally distributed error. The solid curves in the side-panels of Figure 1 show the phase distribution that results from the above eccentricity dispersion, using the observed values of  $\Delta$ . The dependence of the total likelihood on  $\sigma_e$  is shown in Figure 2.

Figure 3 shows the distributions of TTV phases for large and small planets separately, taking  $2.5R_\oplus$  as the dividing line between large and small.<sup>9</sup> Larger planets tend to have smaller phases, which are indicative of lower eccentricities. To be quantitative, the phase distribution of pairs of large planets differs from that of small planets at 97% confidence, based on a K-S test of the absolute phases. Fitting for the eccentricity distributions of the two subsamples separately, we find that the large planets are around half as eccentric, with eccentricity

<sup>7</sup> We define the TTV phase as  $\phi = \angle(V \times \text{sgn}\Delta)$  for the inner planet, and the same for the outer (Lithwick et al. 2012). The extra factor of  $\text{sgn}\Delta = \pm 1$  allows pairs narrow and wide of resonance to be treated symmetrically.

<sup>8</sup> The Rayleigh distribution is equivalent to a 2D Gaussian  $\propto \exp(-(e_x^2 + e_y^2)/2\sigma_e^2)$  for the real and imaginary parts of the complex eccentricity  $z = e_x + ie_y$ .

<sup>9</sup> We detail below how we infer planet radii.



**Figure 2.** The dependence of the total likelihood of observed TTV phases on the eccentricity dispersion. The vertical axis is the decrease in log-likelihood relative to its maximum. Separate curves are shown for all planet pairs (black), large planet pairs with  $R \ \& \ R' > 2.5R_\oplus$  (blue), and small planet pairs with  $R \ \& \ R' < 2.5R_\oplus$  (green). Dashed horizontal lines indicate decreases in  $\ln \mathcal{L}$  of  $-0.5$ ,  $-2$ , and  $-4.5$  which correspond to nominal 1, 2, and 3 $\sigma$  confidence limits.

dispersions given by

$$\sigma_e = \begin{cases} 0.017_{-0.005}^{+0.009}, & \text{for } R \ \& \ R' < 2.5R_\oplus \\ 0.008_{-0.002}^{+0.003}, & \text{for } R \ \& \ R' > 2.5R_\oplus \end{cases}, \quad (5)$$

The best-fit phase distributions corresponding to these  $\sigma_e$  are plotted in Figure 3.

A potential concern is that smaller planets tend to have more uncertain transit times because their transit signal is weaker. Hence their broader distribution of TTV phases could be due to measurement error. Nonetheless, we feel it likely that smaller planets are truly more eccentric, both because the error bars in Eq. (5) seem sufficiently small to distinguish the two groups, and because another indicator of eccentricity—the nominal densities (see below)—also supports this conclusion. An additional concern is that higher eccentricities boost the TTV signal, making it easier to detect. So while the  $\sigma_e$  we report for small planets with detected TTV's might be correct, we are biased against planets with smaller  $e$ . The same concern does not apply to the large planets because they have  $\sigma_e \lesssim |\Delta|$ , and hence most cannot have much of a boost. A more careful investigation of the underlying distributions must await future investigation.

### 3.2. Planet Masses and Densities

The masses are encoded in the absolute values of  $V$  and  $V'$ . We define the nominal mass as the mass that would be inferred if one assumed (incorrectly, in general) that the (free) eccentricity vanishes,

$$\begin{aligned} m_{\text{nom}} &= M_* \left| \frac{V'\Delta}{P'g} \right| \pi j \\ m'_{\text{nom}} &= M_* \left| \frac{V\Delta}{Pf} \right| \pi j^{2/3} (j-1)^{1/3} \end{aligned} \quad (6)$$

(Eqs. (2)). Since eccentricities do not vanish in general, the true mass  $m$  differs from the nominal one by an eccentricity-dependent factor:

$$m = \frac{m_{\text{nom}}}{|1 - 3Z_{\text{free}}^*/(2g\Delta)|} \quad (7)$$

with an analogous expression for  $m'$ . If planets in a pair have very low eccentricities ( $e \ll |\Delta|$ ), the nominal masses are the true masses, whereas if the eccentricities are much higher than that ( $e \gg |\Delta|$ ), the nominal masses

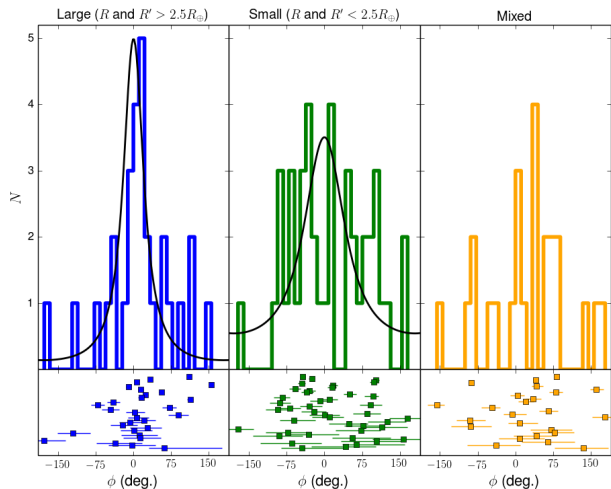


**Figure 3.** Histograms of inner-planet TTV phases of the large ( $R$  and  $R' > 2.5R_{\oplus}$ ), small ( $R$  and  $R' < 2.5R_{\oplus}$ ), and mixed (one large, one small) planet pairs. In the lower panels, the individual phases are shown. The phases of the large planets are more concentrated around  $0^{\circ}$ , indicating they have smaller eccentricities. The phase distributions resulting from the best-fit  $\sigma_e$  (Eq. 5) are plotted as solid curves after folding in the observed values of  $\Delta$ .

are overestimates of the true masses. For intermediate eccentricities ( $e \sim |\Delta|$ ), the nominal and true masses differ by an order unity factor—they can be either smaller or larger depending on the phase of  $Z_{\text{free}}$ .

Table 2 lists the nominal masses of the planets in our primary sample, and the top panel of Figure 4 plots these against planet radii. For planets with multiple TTV partners, we use the TTV amplitude with the smallest fractional uncertainty to compute its nominal mass. The quoted error on nominal mass combines the 68%-confidence error in TTV amplitude with that in stellar mass. To determine planet radii and stellar host parameters, we take star masses and radii from Huber et al. (2013), as listed at the NASA Exoplanet Archive<sup>10</sup>. We obtain planet radius by multiplying the star’s radius by the planet-to-star size ratio reported on the Exoplanet Archive; the latter come from the literature if available, and otherwise from the Kepler pipeline. There are 11 host stars among our primary sample for which Mann et al. (2013) have published revised parameters based on spectroscopic models calibrated to nearby late K and M-dwarfs. We use their values of stellar radius and mass along with planet radii where applicable.

In order to focus on pairs that likely have small eccentricities, and thus true masses close to their nominal masses, we split our sample into “low- $e$ ” and “high- $e$ ” planets. A pair is categorized as high- $e$  if it satisfies any of the following criteria:

1. The TTV phase differs, at 68% confidence, by more than  $30^{\circ}$  from its zero- $e$  value, i.e., from  $0^{\circ}$  for the inner planet or  $180^{\circ}$  for the outer, using whichever planet has the smaller phase error.
2. The nominal density exceeds that of pure iron composition at 68% confidence. Since true densities are likely not so high, these planets presumably have

large  $e$  and hence a large correction to their nominal masses. This conjecture is supported by the fact that many planets nominally denser than iron possess large TTV phase (Fig. 4).

3. One or both planets have transit durations that imply  $e > |\Delta|$  at 68% confidence (Fig. 6). This criterion could be triggered by an underestimated radius for the planet’s host star, rather than the planet’s high  $e$ . But for such planets, the nominal density would also exceed the true density.

We find 83 planets fall into the high- $e$  sample, and 56 in the low- $e$  sample. The nominal masses for the latter are shown in the lower panel of Fig. 4, and the nominal densities in Fig. 5.

We determine a mass-radius relationship for the low- $e$  planets<sup>11</sup> by performing a linear least-squares fit in log-log space, yielding

$$m_{\text{nom}} \approx 14.9^{+3.4}_{-2.8} M_{\oplus} \times \left( \frac{R}{3R_{\oplus}} \right)^{0.65 \pm 0.14} \quad (8)$$

The nominal masses likely exceed the true masses by a modest amount for the low- $e$  sample. Applying the statistical correction procedure described in Wu & Lithwick (2013), we estimate that the correction factor to the best fit is  $\lesssim 10\%$ , and hence we ignore it. Converted to densities, the above fit implies

$$\rho_{\text{nom}} \approx 3 \text{ g/cm}^3 \times (R/3R_{\oplus})^{-2.3}. \quad (9)$$

This agrees reasonably well with what was found in Wu & Lithwick (2013) based on a smaller sample of TTV’s. It is also in adequate agreement with results from planets with RV-determined masses (Fig. 5), which were not included in the fit. Weiss & Marcy (2014) report  $m \approx 7 M_{\oplus} \times (R/3R_{\oplus})^{0.93}$ , for planets in the size range  $1.5R_{\oplus} < R < 4R_{\oplus}$ , based primarily on RV measurements.

Large planets ( $> 2.5R_{\oplus}$ ) appear to be distinct from small ones ( $< 2.5R_{\oplus}$ ) in a number of ways. First, larger planets tend to be less dense. Many large ones are less dense than water, indicating that their radii must be set to a large extent by a gaseous hydrogen atmosphere. By contrast, nearly all small ones are denser than water, and some are even denser than rock. Second, small ones tend to be closer to their star: the median orbital period for small planets in our primary sample is 10.1 d, whereas that of the large ones is 15.3 d. Such a correlation for Kepler candidates has been noted in Wu & Lithwick (2013) and Owen & Wu (2013). As argued there, all planets might have started out with gaseous envelopes, and then the ones closer to their star were photoevaporated. However, this correlation could also be owed, at least partially, to biases in transit detectability (Gaidos & Mann 2013). We also find here modest evidence that closer-in planets are denser (Fig. 7).

And third, as shown above, small ones are around twice as eccentric (Eq. 5; Fig. 3). This is corroborated by the fact that planets in Fig. 4 with nominal densities higher than iron have  $R < 2.5R_{\oplus}$ .

<sup>10</sup> <http://exoplanetarchive.ipac.caltech.edu/index.html>

<sup>11</sup> We exclude Kepler-51c (KOI620.03) from our mass-radius fits, as it is significantly larger than the other planets ( $9.3R_{\oplus}$ ).

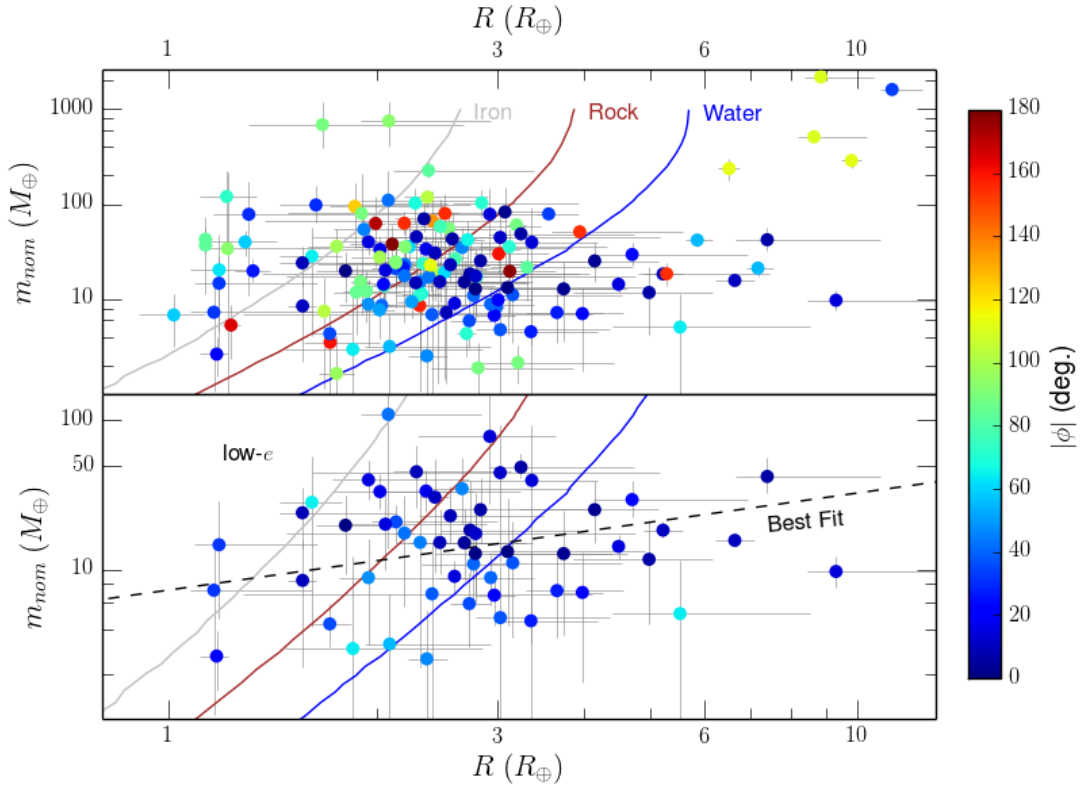


**Figure 4.** Nominal planet mass versus radius. The top panel is the full primary sample, and the lower panel shows the low- $e$  subsample, for which the nominal mass is likely close to the true mass. The best fit relation is given by Eq. 8. Colors signify the TTV phase which we take to be either  $\phi$  or  $\phi' - 180^\circ$ , depending on which planet in a pair has the smaller phase error bar. Colored curves are theoretical mass-radius relations for pure compositions of iron (grey), rock (brown), and water (blue) from Fortney et al. (2007). Note the y-axis scales are different in the top and bottom panels.

It would be of interest to know whether *Kepler* planets are mostly water. If so, it would suggest that the planets formed beyond the ice-line and then migrated inwards; if not, it would argue for *in situ* formation. Unfortunately, the water content is difficult to deduce, since the density is very sensitive to the presence of hydrogen; e.g., a  $5M_\oplus$  rocky planet with a hydrogen atmosphere that is only  $\sim 1\%$  of its mass would have the same density as a pure water planet (Adams et al. 2008; Wu & Lithwick 2013). But we conjecture that the majority of planets are nearly water-free, based on the fact that planets of a given mass span such a wide range of densities—from less dense than water to denser than rock, without much evidence for a pileup of planets near the water-density curve. Furthermore, the fact that small planets tend to be closer to their star suggests that those might have lost their gaseous envelope by photoevaporation, exposing the rocky core underneath (Lopez et al. 2012; Wu & Lithwick 2013; Owen & Wu 2013).

#### 4. SUMMARY

We have extracted the eccentricities and masses—and hence densities—of a large sample of *Kepler* planets, starting from the Mazeh et al. (2013) catalog of transit times through Quarter 12. We found 139 planets suitable for our analysis. In order to invert the observed TTVs, we used an analytical formula for the TTVs of near-resonant pairs. Inverting the analytical formula is not only much faster than the more typically used N-body inversion (Holman et al. 2010; Lissauer et al. 2011b;

Cochran et al. 2011; Lissauer et al. 2013), but it also allows one to break the strong degeneracy between mass and eccentricity in a statistical way. We largely followed the approach of Lithwick et al. (2012); Wu & Lithwick (2013), but applied it to a significantly larger sample and for nearly twice the duration. Our main results are as follows.

- From the TTV phases, the planets' eccentricities are of order a few percent, with r.m.s.  $\sigma_e = 0.018^{+0.005}_{-0.004}$ , when fit with a Rayleigh distribution. Small planets ( $< 2.5 R_\oplus$ ) are around twice as eccentric as the larger ones.
- The nominal masses—and hence densities—were extracted from the TTV amplitudes. The nominal densities of the low- $e$  planets, which are expected to be comparable to the true planet densities, are displayed in Fig. 5 (see also Table 2). The mass-radius relation we infer from TTV's largely agrees with that found from RV. Large planets ( $> 2.5 R_\oplus$ ) appear distinct from small ones, in that many of them are so underdense that they must be covered in gas, whereas most small ones are as dense as water or rock. In addition, the large ones are typically less eccentric and further from their host star.

The untimely malfunction of the *Kepler* satellite makes it unlikely that the number of planets with TTV-measured eccentricities and densities will increase substantially in the near future. But there are a number of

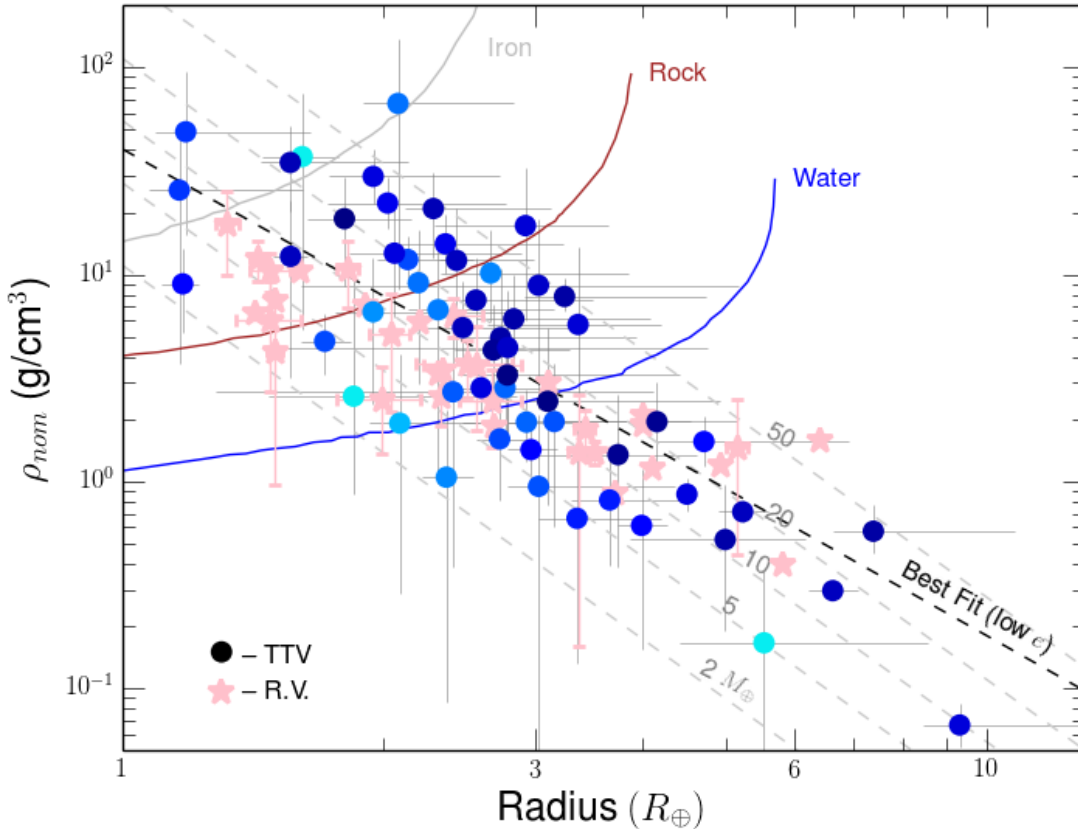


**Figure 5.** Nominal planet density versus radius for the 56 planets in our low- $e$  sample. These planets likely have true densities  $\rho \approx \rho_{nom}$ . The color scheme for the circles is as described in Figure 4. The best fit relation is plotted as a black dashed line (Eq. 9). Pink stars are planets with RV-determined masses, including those listed in Table 3 of Wu & Lithwick (2013), Kepler planets listed in Table 2 of Marcy et al. (2014), as well as Kepler-68c (Gilliland et al. 2013), and HD97658b (Dragomir et al. 2013).

prospects for improving upon the results of this paper. First, *Kepler* has released lightcurves up to Quarter 16, and the present study may be extended to incorporate them. Second, the radii of stars in the Kepler catalog are uncertain. This directly translates into uncertainty in the planet radii—and hence densities. For a crude estimate of the error, we compare the radii of the 38 stars in our primary sample that have been followed up (e.g., with spectroscopy or asteroseismology) with their pre-follow-up values, and find that the median error is 12%; 31 of the stars have errors < 25%, but three have errors larger than 50%. In the future, more accurate measurements of stellar radii will yield more accurate planet densities.

Third, the TTV signals sometimes have components in addition to the dominant one of Eq. (1), especially when a planet pair lies near a higher-order resonance. If these are detected and decoded, they can be used to help break the mass-eccentricity degeneracy. And fourth, RV measurements will continue to expand our knowledge of sub-Jovian planets.

#### ACKNOWLEDGMENTS

We thank Will Farr, Eric Gaidos, Jason Steffen, and Yanqin Wu for helpful discussions. We are also grateful to the *Kepler* team for acquiring and publicly releasing such spectacular results. YL acknowledges support by NSF Grant AST-1109776 and NASA grant NNX14AD21G.

#### REFERENCES

- Adams, E., Seager, S., & Elkins-Tanton, L. 2008, *The Astrophysical Journal*, 673, 1160
- Agol, E., Steffen, J., Sari, R., & Clarkson, W. 2005, *Monthly Notices of the Royal Astronomical Society*, 359, 567
- Batalha, N. M., Borucki, W. J., Bryson, S. T., et al. 2011, *The Astrophysical Journal*, 729, 27
- Batalha, N. M., Rowe, J. F., Bryson, S. T., et al. 2013, *The Astrophysical Journal Supplement Series*, 204, 24
- Borucki, W. J., Koch, D., Basri, G., et al. 2010, *Science*, 327, 977
- Borucki, W. J., Koch, D. G., Basri, G., et al. 2011, *The Astrophysical Journal*, 736, 19
- Cochran, W. D., Fabrycky, D. C., Torres, G., et al. 2011, *The Astrophysical Journal Supplement Series*, 197, 7
- Dragomir, D., Matthews, J. M., Eastman, J. D., et al. 2013, *ApJ*, 772, L2
- Fabrycky, D. C., Ford, E. B., Steffen, J. H., et al. 2012, *The Astrophysical Journal*, 750, 114
- Fang, J., & Margot, J.-L. 2012, *The Astrophysical Journal*, 761, 92
- Figueira, P., Marmier, M., Boué, G., et al. 2012, *A&A*, 541, A139
- Ford, E. B., Quinn, S. N., & Veras, D. 2008, *The Astrophysical Journal*, 678, 1407
- Fortney, J., Marley, M., & Barnes, J. 2007, *The Astrophysical Journal*, 659, 1661
- Gaidos, E., & Mann, A. W. 2013, *The Astrophysical Journal*, 762, 41
- Gautier, III, T. N., Charbonneau, D., Rowe, J. F., et al. 2012, *The Astrophysical Journal*, 749, 15
- Gilliland, R. L., Marcy, G. W., Rowe, J. F., et al. 2013, *The Astrophysical Journal*, 766, 40
- Holman, M. J., & Murray, N. W. 2005, *Science*, 307, 1288

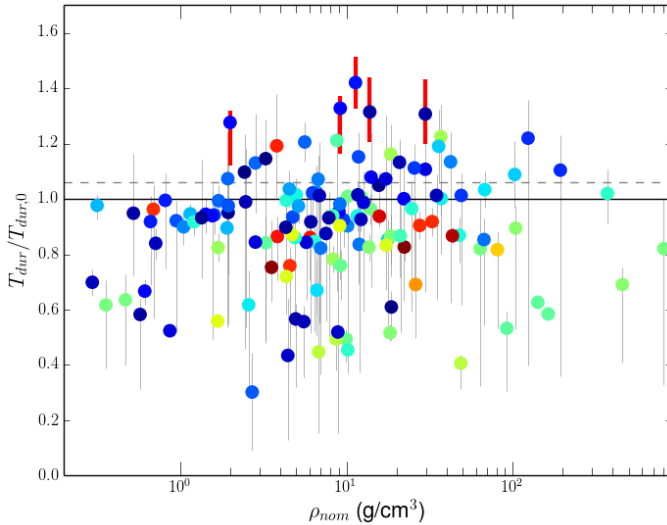


**Figure 6.** Selecting high- $e$  planets based on transit duration. The x-axis shows the planets' nominal density, and the y-axis shows the ratio of their observed transit durations to what the duration would be if the planet were on a circular orbit with zero impact parameter. When that ratio exceeds unity, the eccentricity is bounded from below by  $e > T_{\text{dur}}/T_{\text{dur},0} - 1$  (Eq. 1 of Ford et al. 2008, to linear order in  $e$ ). The dashed line corresponds to a minimum eccentricity of 0.06, which is greater than 99.7% of eccentricities belonging to our best-fit eccentricity distribution. The color/symbol scheme is as described in Fig. 4. Error bars are based on uncertainty in stellar radius, and are suppressed in the x-direction. Five planets are selected as high- $e$  based on transit duration alone and are emphasized with bold red error bars. In addition, many of the planets selected as high- $e$  based on TTV phase or nominal density also have large transit durations, corroborating their membership in the high- $e$  sample.

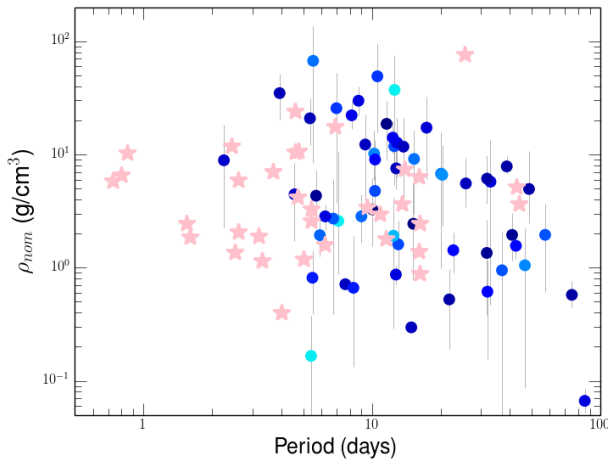


**Figure 7.** Nominal planet density of the low- $e$  subsample versus orbital period. The color and symbol scheme is the same as described in Fig. 4. While planet densities are quite scattered, there is a hint of closer-in planets being denser. The RV planets probe significantly shorter periods than the majority of TTV planets.

- Holman, M. J., Fabrycky, D. C., Ragozzine, D., et al. 2010, *Science*, 330, 51
- Huber, D., Aguirre, V. S., Matthews, J. M., et al. 2013, arXiv preprint arXiv:1312.0662
- Johansen, A., Davies, M. B., Church, R. P., & Holmelin, V. 2012, *The Astrophysical Journal*, 758, 39
- Koch, D. G., Borucki, W. J., Rowe, J. F., et al. 2010, *The Astrophysical Journal Letters*, 713, L131
- Lissauer, J. J., Ragozzine, D., Fabrycky, D. C., et al. 2011a, *The Astrophysical Journal Supplement Series*, 197, 8
- Lissauer, J. J., Fabrycky, D. C., Ford, E. B., et al. 2011b, *Nature*, 470, 53
- Lissauer, J. J., Jontof-Hutter, D., Rowe, J. F., et al. 2013, *The Astrophysical Journal*, 770, 131
- Lithwick, Y., Xie, J., & Wu, Y. 2012, *The Astrophysical Journal*, 761, 122
- Lopez, E. D., Fortney, J. J., & Miller, N. 2012, *The Astrophysical Journal*, 761, 59
- Mann, A. W., Gaidos, E., & Ansdell, M. 2013, *The Astrophysical Journal*, 779, 188
- Marcy, G. W., Isaacson, H., Howard, A. W., et al. 2014, *The Astrophysical Journal Supplement Series*, 210, 20
- Mazeh, T., Nachmani, G., Holczer, T., et al. 2013, *ApJS*, 208, 16
- Nesvorný, D., Kipping, D. M., Buchhave, L. A., et al. 2012, *Science*, 336, 1133
- Owen, J. E., & Wu, Y. 2013, *ApJ*, 775, 105
- Steffen, J. H., Fabrycky, D. C., Ford, E. B., et al. 2012, *Monthly Notices of the Royal Astronomical Society*, 421, 2342
- Steffen, J. H., Fabrycky, D. C., Agol, E., et al. 2013, *Monthly Notices of the Royal Astronomical Society*, 428, 1077
- Tremaine, S., & Dong, S. 2012, *The Astronomical Journal*, 143, 94
- Weiss, L. M., & Marcy, G. W. 2014, *The Astrophysical Journal Letters*, 783, L6
- Weissbein, A., Steinberg, E., & Sari, R. 2012, arXiv preprint arXiv:1203.6072
- Wu, Y., & Lithwick, Y. 2013, *ApJ*, 772, 74
- Xie, J.-W. 2013, *ApJS*, 208, 22
- Xie, J.-W. 2014, *The Astrophysical Journal Supplement Series*, 210, 25

**Table 1**  
TTV Amplitudes

KOI in/out	$P$ (d)	$P'$ (d)	$j$	$\Delta$	$ V $ min.	$ V' $ min.	$\phi$ deg.	$\phi'$ deg.
82.02/01	10.31	16.15	3	0.044	—	$1.4^{+0.5}_{-0.5}$	—	$159^{+25}_{-25}$
82.04/02	7.07	10.31	3	-0.028	$16.0^{+5.8}_{-5.8}$	—	$10^{+19}_{-17}$	—
85.01/03	5.86	8.13	4	0.041	$0.2^{+3.6}_{-0.2}$	$4.1^{+2.8}_{-2.8}$	$-33^{+180}_{-180}$	$-102^{+38}_{-45}$
111.01/02	11.43	23.67	2	0.036	$1.1^{+2.3}_{-1.1}$	$3.3^{+2.1}_{-2.1}$	$5^{+180}_{-180}$	$2^{+42}_{-43}$
115.01/02	5.41	7.13	4	-0.013	$1.3^{+3.0}_{-0.8}$	$3.1^{+2.5}_{-2.5}$	$-148^{+103}_{-46}$	$-116^{+54}_{-52}$
137.01/02	7.64	14.86	2	-0.028	$5.3^{+0.4}_{-0.4}$	$4.1^{+0.3}_{-0.3}$	$-8^{+5}_{-5}$	$170^{+5}_{-5}$
148.01/02	4.78	9.67	2	0.012	$4.0^{+1.2}_{-1.2}$	$3.1^{+0.8}_{-0.8}$	$-6^{+16}_{-16}$	$-159^{+16}_{-16}$
152.02/01	27.40	52.09	2	-0.050	$1.0^{+4.0}_{-1.0}$	$5.7^{+1.3}_{-1.3}$	$17^{+180}_{-180}$	$-99^{+14}_{-13}$
152.03/02	13.48	27.40	2	0.016	$8.2^{+2.8}_{-2.8}$	$21.7^{+3.9}_{-3.9}$	$-36^{+17}_{-18}$	$135^{+8}_{-8}$
156.01/03	8.04	11.78	3	-0.024	$1.3^{+1.4}_{-1.3}$	$3.3^{+0.7}_{-0.7}$	$-5^{+180}_{-180}$	$150^{+12}_{-12}$
...	...	...	...	...	...	...	...	...

**Note.** — Table 1 is published in its entirety in the electronic edition of ApJ. A portion is shown here for guidance. Each line gives the TTV amplitudes for the inner and outer member of a pair of interacting planets, obtained by fitting the transit times catalogued in Mazeh et al. (2013). The TTV amplitudes (complex numbers  $V$  and  $V'$ ) are denoted here by their magnitudes ( $|V|$  and  $|V'|$ ) and phases ( $\phi$  and  $\phi'$ ), with error bars at 68% confidence. Our primary sample consists of planets whose TTV magnitudes are inconsistent with zero within the error bar. In other columns,  $P$  and  $P'$  are orbital periods,  $j$  is the nearest  $j:j-1$  resonance, and  $\Delta$  is the normalized distance to resonance. Dashes appear for middle planets in degenerate triples (see footnote 5).

**Table 2**  
Planet Nominal Masses

Planet	$m_{\text{nom}}^{\text{a}}$ ( $M_{\oplus}$ )	$R_p$ ( $R_{\oplus}$ )	$e$ -flag <sup>b</sup> (h/l)	$M_*$ ( $M_{\odot}$ )	$R_*$ ( $R_{\odot}$ )
82.02	$2.6^{+1.3}_{-1.1}$	$1.2^{+0.1}_{-0.1}$	l	0.73	0.755
85.01	$26.6^{+20.4}_{-18.5}$	$2.6^{+0.04}_{-0.04}$	h	1.27	1.424
111.01	$19.6^{+14.5}_{-12.4}$	$3.1^{+0.5}_{-0.7}$	h	0.81	1.361
115.01	$5.1^{+6.3}_{-4.1}$	$5.5^{+3.0}_{-1.1}$	l	1.09	1.332
115.02	$3.0^{+9.2}_{-2.0}$	$1.9^{+1.0}_{-0.4}$	l	1.09	1.332
137.01	$18.4^{+2.7}_{-1.9}$	$5.2^{+0.4}_{-0.3}$	l	0.88	1.055
137.02	$15.7^{+2.0}_{-1.4}$	$6.6^{+0.5}_{-0.4}$	l	0.88	1.055
148.01	$14.3^{+4.3}_{-4.5}$	$2.0^{+0.2}_{-0.1}$	h	0.96	0.852
148.02	$9.8^{+3.3}_{-3.4}$	$3.0^{+0.4}_{-0.1}$	h	0.96	0.852
152.02	$13.7^{+6.5}_{-4.5}$	$2.0^{+0.9}_{-0.2}$	h	1.08	1.037
...	...	...	...	...	...

**Note.** — Table 2 is published in its entirety in the electronic edition of ApJ. A portion is shown here for guidance.

<sup>a</sup> Planet nominal mass, given by Eq. (6)

<sup>b</sup> Flag indicating whether the planet is classified as high- $e$  (“h”) or low- $e$  (“l”) according to criteria listed in Section 3.2